*Polymer Engineering & Science*

WILEY | spe INSPIRING PLASTICS PROFESSIONALS

RESEARCH ARTICLE OPEN ACCESS

# Viscosity Reduction in Diluted Polyethylene Melts: A Comparative Study of Semiempirical, Viscoelastic, and Equation-of-State Modeling Frameworks

Ernst Georg Viehböck[1,2] | Alexander Hammer[2] | Markus Kirchmayr[3] | Christof Murnig[4] | Christian Paulik[1,5] | Gerald Berger-Weber[2]

[1]Competence Center CHASE GmbH, Linz, Austria | [2]Institute of Polymer Processing and Digital Transformation, Johannes Kepler University Linz, Linz, Austria | [3]EREMA Engineering Recycling Maschinen Und Anlagen Ges.M.B.H, Ansfelden, Austria | [4]GAW Technologies GmbH, Graz, Austria | [5]Institute of Chemical Technology of Organic Materials, Johannes Kepler University Linz, Linz, Austria

**Correspondence:** Ernst Georg Viehböck (ernst.viehboeck@chasecenter.at)

**Received:** 20 December 2025 | **Revised:** 26 January 2026 | **Accepted:** 13 February 2026

**Keywords:** diluted melts | extrusion | in-line rheometry | polymer recycling | supercritical fluids | time-concentration superposition | viscosity modeling

## ABSTRACT

Accurate prediction of viscosity reduction is a prerequisite for optimizing advanced polymer recycling and processing technologies, particularly, when dealing with complex fluids such as postconsumer (PCRs) or diluted melts. This study presents a comprehensive rheological framework characterizing the flow behavior of high-density polyethylene (PE-HD) and low-density polyethylene PCR diluted with *n*-decane (C10), a specialty recycling solvent from the CreaSolv-technology (CS), and supercritical carbon dioxide ($CO_2$) using an in-line slit-die rheometer. By systematically evaluating three modeling approaches of increasing physical depth, we bridge the gap between fundamental thermodynamics and practical process control. While parallel-plate rheometry confirmed the absence of wall slip in the investigated shear rate regime, the modeling analysis revealed distinct trade-offs between physical fidelity and predictive capability. A semiempirical model utilizing an exponential (Arrhenius-like) concentration term demonstrated good performance for the observed diluent concentration regime, achieving mean relative errors for all diluent systems below 5%. In contrast, a fundamental approach coupling the Sanchez–Lacombe Equation of State (EOS) with the Kelley–Bueche theory successfully validated the functional form of dilution but consistently underestimated the magnitude of viscosity reduction. Ultimately, this work derives a physically validated, four-parameter semiempirical model that eliminates the need for complex molecular weight data as needed for the reptation-based Schausberger model, enabling the direct integration of rheological predictions for variable PCR feedstocks into digital twins and real-time process optimization tools.

## 1 | Introduction

Accurate prediction of polymer melt viscosity is essential for the design and optimization of polymer processing methods, such as extrusion, injection molding, and polymer foaming. In industrial practice, low-molecular-weight diluents are frequently used to decrease viscosity and thus facilitate material handling and reduce the energy required for melt transport. Lower melt viscosity translates into decreased pressure levels within dies, molds, and filter systems, which minimizes mechanical stress on equipment and material degradation due to dissipation while enabling higher throughput at reduced specific energy input. These benefits are, particularly, relevant in systems such as polyvinyl chloride (PVC), where plasticizers are routinely employed to achieve processable viscosities and decrease mechanical stiffness for applications such as shoes and calendered films [1, 2]. Additionally, viscosity reduction is a prerequisite for thermoplastic foaming, as it supports

**Highlights**

- In-line rheometry of diluted polyethylene melts.
- Comparison of three distinct viscosity modeling approaches.
- Application of time-concentration superposition principles.
- Development of a robust semiempirical model for viscosity prediction.
- Validation of the final model against a physically based framework.

efficient cell nucleation and expansion at practical pressures, particularly, when physical blowing agents such as $CO_2$ or $N_2$ are used [3].

Although neat polymer rheology has been studied extensively, the superposition of and interaction of shear rate, temperature, pressure, and diluent concentration on viscosity remain insufficiently characterized, in particular, in systems with complex compositions, for instance, postconsumer recyclates or nonstandard solvents. This challenge is compounded when thermodynamic properties such as solubility, density, phase behavior, or particular interaction parameters of the diluents used are unknown or difficult to access [4].

### 1.1 | Approaches to Modeling Viscosity Reduction

Various modeling approaches have been developed to capture the effects of dilution on polymer viscosity. Many of these are grounded in free-volume theory, which postulates that adding a diluent increases the fractional free volume available in the polymer matrix, thereby enhancing chain mobility, analogous to the effect of raising temperature [2]. Early models, such as the Doolittle equation, capture the exponential dependence of viscosity on free volume, while extensions by Kelley and Bueche allow for prediction in polymer–solvent systems by averaging component free volumes [5]. Fujita and Kishimoto further refined this by linking concentration shift factors directly to changes in fractional free volume [6, 7].

The methodological foundation for time-concentration superposition (TCS) was laid by Schausberger, Knoglinger, Kastner, and Janeschitz-Kriegl [8–10]. Their approach rests on the premise that the complex rheological changes induced by a diluent can be methodologically decoupled into two independent physical contributions. By isolating the topological effect, specifically the reduction of entanglement density as a vertical scaling, and separately treating the enhanced chain mobility (changes in monomeric friction and free volume) as a horizontal scaling, they established a robust protocol for data unifications [11].

Building upon these foundational concepts, subsequent research extended the scaling methodologies to more complex systems, such as gas-swollen melts [12] or high-pressure $CO_2$ systems incorporating glass transition temperature ($T_g$) depression [13]. More recently, Park and Dealy demonstrated the separability of pressure and concentration effects [14, 15], and Schaible and Bonten applied these principles to in-line foam injection molding [16].

Parallel to scaling, advanced frameworks combine rheological models with equations of state (EOS), such as the Sanchez–Lacombe EOS (S-L EOS) [17]. By coupling the S-L EOS with rheological models, such as the Cross–Carreau formulation or the Kelley–Bueche equation, researchers have successfully predicted the concentration-dependent viscosity behavior of various polymer/gas systems from first principles [12, 14, 18, 19].

### 1.2 | Scope of This Work

In light of these challenges, purely empirical and semiempirical approaches remain attractive alternatives, offering broader applicability and reduced reliance on detailed thermodynamic input [20–22]. This study aims to bridge the gap between rigorous thermodynamic modeling and practical process characterization. We present a comprehensive investigation of viscosity reduction in polyethylene melts diluted with standard alkanes, specialty solvents, and physical blowing agents ($CO_2$). To describe the rheological behavior, we compare three modeling approaches of increasing physical depth, which are detailed in Section 3: (i) a compact semiempirical model, (ii) the viscoelastic Schausberger model (TCS), and (iii) a thermodynamic prediction derived from the S-L EOS and the Kelley–Bueche framework.

## 2 | Experimental

In order to validate the theoretical concepts and modeling approaches discussed in the preceding section, experimental investigations were conducted on selected polymer–diluent systems under processing-relevant conditions. The experimental setup was designed to enable the controlled injection of low-molecular-weight diluents into pressurized polymer melts and thus facilitate systematic evaluation of viscosity reduction.

### 2.1 | Materials

To systematically investigate the reduction of viscosity in polymer and diluent systems, a set of materials was selected.

The polymeric base material used in this study was a high-density polyethylene (PE-HD) grade BB2581 (Borealis, Vienna, Austria), which was designed specifically for blow-molding applications, and has a multimodal molecular weight distribution, a melt flow rate (MFR) of 0.3 g/10 min (190°C, 2.16 kg) and a melt density of 0.746 $g/cm^3$ at 200°C.

To broaden the investigation beyond virgin materials and to evaluate the applicability of the approach to recycling processes, a post-consumer recyclate was included. The recycled material, predominantly low-density polyethylene (PE-LD PCR), was

sourced from a commercial recycling process and shows an MFR of 1.70 ± 0.03 g/10 min (200°C, 5 kg) and a melt density of 0.754 g/cm$^3$ at 200°C.

For dilution of the polymer melts, three diluent systems were used. First, *n*-decane (C10; purity >99%, Sigma Aldrich), a low-molecular-weight (142.28 g/mol) linear alkane, was selected due to its chemical compatibility with polyethylene. Second, a specialty solvent from the CreaSolv-process (CS) (CreaCycle, Grevenbroich, Germany) was employed as a benchmark to compare the effects on viscosity reduction of an advanced and of a pure hydrocarbon diluent. Finally, carbon dioxide ($CO_2$; purity ≥ 99.9%, Linde Gas GmbH, Austria) was utilized as a physical blowing agent to investigate the rheological behavior of gas-loaded melts.

The polymer–diluent combinations investigated are summarized in Table 1.

## 2.2 | Experimental Setup

The experimental setup, see more details in Viehböck et al. [23], is based on a single-screw extruder equipped with an integrated slit rheometer and a dedicated diluent injection system. As illustrated in Figure 1, a high-performance liquid chromatography (HPLC) pump was used to inject the diluent directly into the extruder barrel. To enable the characterization of physical blowing agents, this pump can be interchanged with the gas dosing station described previously, utilizing the same injection port to introduce gases such as $CO_2$ or $N_2$.

In this upstream injection configuration, the diluent is forced into the polymer melt during melt conveying to ensure mixing along the screw before the diluted melt enters the rheological measurement section. The injection port can be placed flexibly to target specific zones along the screw and enable systematic investigation of how injection location influences mixing quality and therefore viscosity reduction. Due to the excellent mixing performance achieved in the extruder, the injection position was set closely upstream of the metering zone. All measurements presented in this study were conducted using this injection configuration.

**TABLE 1** | Investigated polymer–diluent combinations.

| Polymer | C10 | CS | $CO_2$ |
|---|---|---|---|
| PE-HD | ✓ | ✓ | |
| PE-LD PCR | | ✓ | ✓ |

The PE-HD was processed using a laboratory-scale single-screw extruder (Thermo Fisher Scientific, Waltham, MA, USA) with a screw diameter of 19 mm and a processing length of 33 times the diameter (33D). The screw had a conventional three-zone design with a smooth-walled barrel and access ports positioned at 13D, 16D, 19D, 21D, 25D, and 33D for integration of pressure and melt-temperature sensors. A water-cooled feed section and an electrically heated barrel enabled thermal management.

Rheology was characterized using an in-line slit-die rheometer with width $W = 20$ mm, height $H = 1.2$ mm, and length $L = 75$ mm. The total slit length was 120 mm, such that both upstream and downstream of the measuring section additional distances were available to decouple the measurement zone from entrance and exit effects. An entrance region ahead (20 mm) of the first transducer ensured absence of entrance effects, while a downstream section of 25 mm provided sufficient distance to ambient pressure at the die exit in order to mitigate bubble nucleation and exclude exit effects. The measuring section itself was instrumented with three pressure transducers located at axial positions of 0, 50, and 75 mm, as well as a melt-temperature sensor positioned at 25 mm.

For injecting liquid diluents into the melt stream, a high-pressure HPLC pump (BlueShadow 40P, Knauer, Berlin, Germany) was employed. This system incorporated a stainless-steel pump head with a nominal flow capacity of 10 mL min$^{-1}$, supporting operation at pressures of up to 65 MPa for flow rates of 4 mL min$^{-1}$, and of up to 40 MPa at 10 mL min$^{-1}$. A downstream nonreturn valve was installed to prevent polymer melt from backflowing into the pump or associated capillary lines.

To investigate the influence of physical blowing agents on the rheological behavior, the experimental setup was extended to allow for the injection of gases such as carbon dioxide ($CO_2$) and nitrogen ($N_2$). A gas dosing station (NC350, Promix Solutions

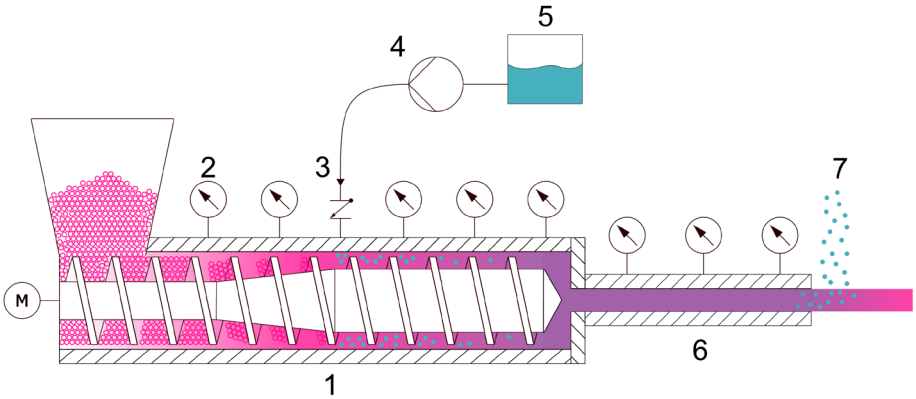


**FIGURE 1** | Schematic overview of the extrusion rheometry setup with injection into the extruder (ER-IS). (1) Single-screw extruder, (2) pressure transducer, (3) check valve, (4) diluent pump or gas dosing station, (5) diluent reservoir, (6) extrusion rheometer, and (7) evaporation of the diluent.

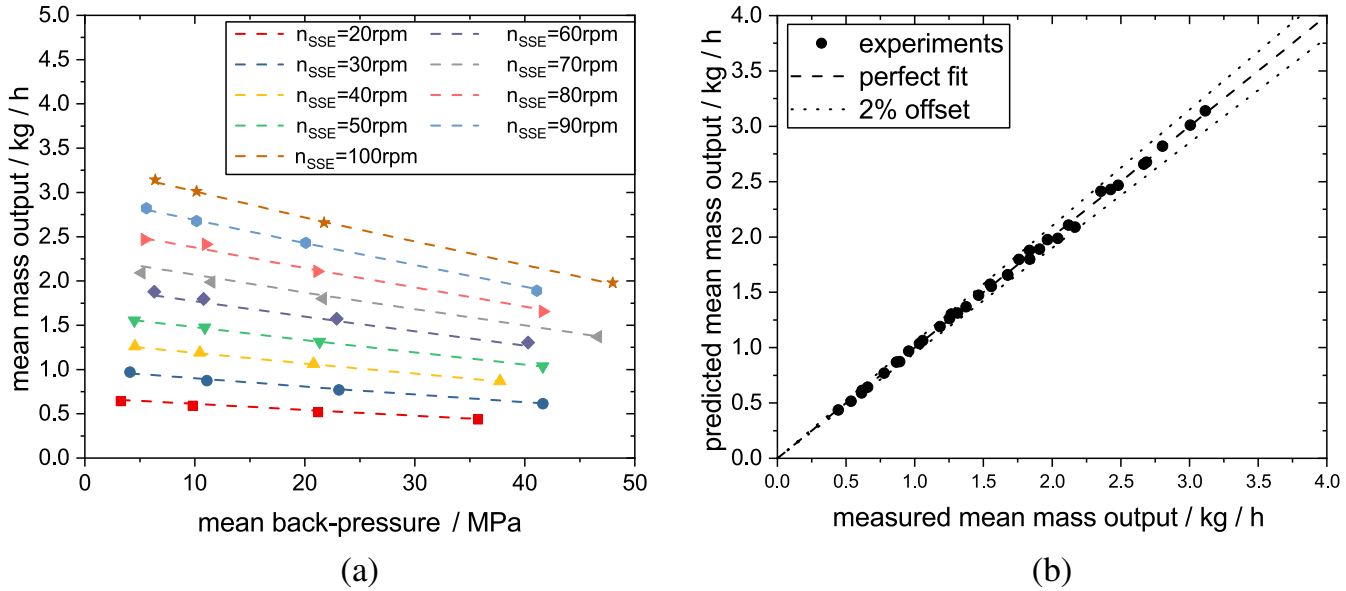


**FIGURE 2** | (a) Screw characteristic curve for PE-HD at 200°C. Dashed lines and symbols show the results of the heuristic model and the experiments, respectively. (b) Measured versus predicted mass output (heuristic model at 200°C). Circles mark the experiments, the dashed line represents a perfect fit of $R^2 = 1$, and the dotted lines indicate a 2% offset from the perfect fit.

AG, Winterthur, Switzerland) was employed for this purpose. This system is equipped with high-pressure pumps capable of compressing the fluids to pressures of up to 35 MPa, enabling them to overcome the melt pressure inside the extruder barrel. To ensure precise dilution levels, the dosing station utilizes integrated mass flow controllers that regulate the gas flow rate independently of process pressure fluctuations. This setup allows for the accurate setting of gas-to-polymer weight fractions, which is critical for the reproducible characterization of the viscosity reduction effects.

### 2.3 | Predicting the Volume Flow

In the ER-IS configuration, the throughput behavior of the single-screw extruder with a smooth intake zone is strongly influenced by the back-pressure applied. Consequently, the volumetric flow rate cannot be directly inferred from the screw rotation speed alone. To address this limitation, a heuristic regression model was developed that predicts the mass output of the extruder based on two key process variables: the screw speed and the back-pressure measured at the screw tip.

We conducted a series of extrusion experiments to generate a comprehensive dataset for model calibration. The screw speed was systematically varied, and the back-pressure was adjusted using a bypass valve to span a broad range of operating conditions. At each material combination, nine distinct screw speeds and, where technically feasible, four different back-pressure levels were tested. To measure the throughput, four independent samples were taken for each combination of parameters, each for a period of 36 s under steady-state extrusion conditions.

The data collected was processed using the open-source symbolic regression platform *HeuristicLab* [24]. Symbolic regression based on evolutionary algorithms was applied to derive an explicit analytical expression for the mass output as a function of screw speed and back-pressure. This approach builds upon earlier work by Marschik et al. [25] and Hammer et al. [26], who demonstrated the applicability of data-driven modeling techniques to polymer processing.

The final models were obtained using the Offspring Selection Genetic Algorithm (OSGA) implemented in HeuristicLab 3.3.16. The algorithmic configuration included a population size of 300, 200 selected parents per generation, one elite per generation, a mutation probability of 20%, and a maximum of 125 generations. The mathematical operations allowed were addition, subtraction, multiplication, division, and exponentiation.

The resulting symbolic regression model, calibrated for PE-HD at 200°C, consists of nine fitted coefficients and exhibits excellent agreement with the experimental data. As illustrated in Figure 2, the model for the screw characteristic line successfully captures the influence of screw speed and back-pressure on mass throughput: subplot (a) presents the modeled versus measured mass throughput, while subplot (b) shows a parity plot that confirms the model's predictive accuracy, with a coefficient of determination $R^2 > 0.99$ and a mean relative error $MRE < 0.33\%$ for both training and validation datasets.

Corresponding model results for additional materials and temperatures are provided in the appendix. Notably, for PE-LD PCR, the model calibrated at 200°C was also used to predict the performance at 240°C, where it achieved excellent generalization, with an $R^2 > 0.994$ on the unseen validation data.

### 2.4 | Prediction of Density Using the S-L EOS

The S-L EOS is used to describe the volumetric behavior of polymer–diluent mixtures [17], which is relevant for converting the

mass throughput of the extruder to the volumetric flow rate required for shear rate calculations in Equation (13). It is formulated in terms of reduced variables and relates the reduced pressure $\widetilde{P}$, the reduced temperature $\widetilde{T}$, and the reduced density $\widetilde{\rho}$:

$$\frac{\widetilde{P}}{\widetilde{T}} = -\ln(1-\widetilde{\rho}) - \left(1-\frac{1}{r}\right)\widetilde{\rho} - \frac{\widetilde{\rho}^2}{\widetilde{T}}. \tag{1}$$

The reduced variables are defined as:

$$\widetilde{T} = \frac{T}{T^*},\ T^* = \frac{\varepsilon^*}{R}, \tag{2}$$

$$\widetilde{P} = \frac{P}{P^*},\ P^* = \frac{\varepsilon^*}{v^*}, \tag{3}$$

$$\widetilde{\rho} = \frac{\rho}{\rho^*},\ \rho^* = \frac{M}{rv^*}, \tag{4}$$

with $T^*$, $P^*$, and $\rho^*$ are the characteristic temperature, pressure, and density; these values are thus independent of variations in pressure and temperature. The symbol $\varepsilon^*$ indicates the characteristic energy of interaction, $v^*$ the characteristic volume for a site in the lattice, and $r$ the number of lattice sites taken up by a molecule with a molecular mass $M$.

For mixtures, the EOS remains formally identical, but mixture parameters must be derived from mixing rules. The average characteristic volume is defined by:

$$v^* = \sum_i \phi_i^\circ v_i^* \tag{5}$$

with the close-packed volume fraction $\phi_i$ of component $i$ given by:

$$\phi_i = \frac{w_i}{\rho_i} \Big/ \sum_i \frac{w_i}{\rho_i}, \phi_i^\circ = \frac{\phi_i P_i^* / T_i^*}{\sum_i \phi_i P_i / T_i} = \frac{\phi_i / v_i^*}{\sum_i \phi_i / v_i^*}. \tag{6}$$

The average number of lattice sites per molecule in the mixture is:

$$r = \sum_i x_i r_i, \tag{7}$$

where $x_i$ is the mole fraction of component $i$ in the mixture. The molecular weight $M$ of the mixture is derived by a linear mixing rule that depends on the molar fraction:

$$M = \sum_i M_i x_i. \tag{8}$$

The characteristic pressure $P^*$ of the mixture is calculated using a geometric mixing rule corrected by a binary interaction parameter $k_{12}$:

$$P^* = \sqrt{P_1^* P_2^*}(1-k_{12}). \tag{9}$$

These mixture parameters enable the computation of reduced thermodynamic variables and, ultimately, of the specific volume $v$ of the polymer–diluent solution.

In practice, the characteristic component parameters ($T^*$, $P^*$, $\rho^*$) required for applying the S-L EOS are typically obtained by fitting the model to experimental PvT data. The binary interaction parameter $k_{12}$, which accounts for nonideal interactions between the components, is most commonly determined from solubility measurements using high-precision techniques, such as magnetic suspension balances [12, 14, 18, 19, 27].

An alternative approach, employed in this study for PE-HD/*n*-decane, is to calibrate $k_{12}$ based on experimentally measured swelling data of polyethylene in *n*-decane as reported by Orwoll and Small [28] for a temperature range from 140°C to 170°C. For each temperature, we determined the corresponding value of $k_{12}$ by fitting the S-L EOS to the swollen volume observed. These temperature-specific values were subsequently extrapolated to the processing-relevant conditions of 200°C and 240°C in the present work.

The fitted results are illustrated in Figure 3, where the S-L EOS was applied with varying $k_{12}$ to reproduce the experimental swelling data.

Each temperature yields a unique best-fit value for $k_{12}$. As suggested by Garg et al., it is often convenient to model $k_{12}$ as a function of temperature [27]. The resulting relationship, for which a linear regression provided an excellent fit with $R^2 > 0.99$, is illustrated in Figure 4 and expressed as:

$$\begin{aligned} k_{12}(T) &= a(T-273.15)+b; \\ a &= 1.332584\times10^{-4}\ \mathrm{K}^{-1}; \\ b &= 8.7033664\times10^{-3}. \end{aligned} \tag{10}$$

This empirical relation was used to estimate $k_{12}$ at the relevant processing temperatures for modeling the behavior of the polymer–diluent mixture.

For the system comprising PE-LD PCR and $CO_2$, the binary interaction parameter $k_{12}$ was determined utilizing the constitutive description provided by Ginting [29]. In his work, a specific temperature-dependent function for $k_{12}$ is defined, which was directly adopted in this study to calculate the interaction parameters required for the S-L EOS under the investigated processing conditions. The model of Ginting is defined as:

$$\begin{aligned} k_{12}(T) &= a\cdot T+b; \\ a &= -1.525\times10^{-3}\ \mathrm{K}^{-1}; \\ b &= 0.5264\times10^{-3}. \end{aligned} \tag{11}$$

It should be acknowledged that the binary interaction parameter $k_{12}$ is possibly sensitive to molecular architecture and branching topology. Consequently, adopting literature data from an unspecified polyethylene grade introduces a degree of uncertainty. However, a sensitivity analysis performed by varying $k_{12}$ values within the range of chemically similar systems revealed that its influence on the predicted mixture density is marginal for the PE/*n*-decane system. This limited sensitivity is attributed to the high thermodynamic compatibility of the components, which exhibit similar densities and chemical structures (aliphatic hydrocarbons) without phase transition under the investigated processing conditions.

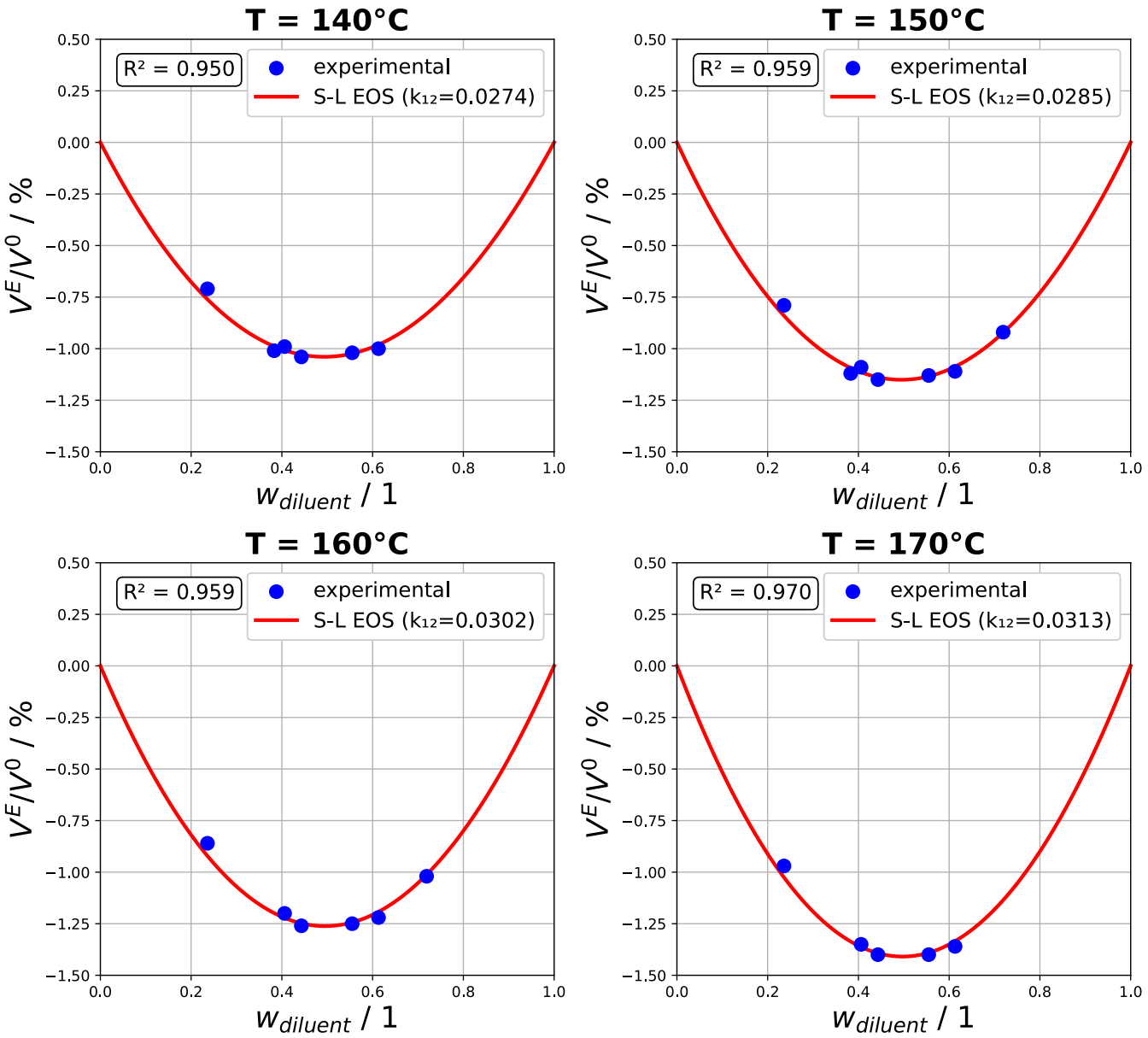


**FIGURE 3** | S-L EOS fit of the excess volume $V^E$ normalized on the ideal (linear) mixing volume $V^0$ for PE/*n*-decane, based on data by Orwoll and Small [28]. The model accurately captures the negative excess volume, confirming nonideal mixing behavior where the mixture density exceeds the linear mixing rule prediction.

### 2.5 | Data Evaluation

Viscosity was determined from slit-die measurements using the Hagen–Poiseuille analogue for rectangular geometries. For a slit of constant cross-section, the wall shear stress $\tau_W$ was obtained from the measured pressure drop $\Delta p$, the slit width $W$, height $H$, and length $L$, with a correction for side-wall effects [30]:

$$\tau_W = \frac{H\Delta p}{2L}\left(1+\frac{H}{W}\right)^{-1}. \tag{12}$$

Reliable viscosity data require fully developed flow, which is indicated by a linear pressure profile along the die length [31]. Under these conditions, effects of viscous heating, pressure dependence of viscosity, or phase separation of the diluent can be neglected.

The apparent shear rate $\dot{\gamma}_{\text{app}}$ was calculated as:

$$\dot{\gamma}_{\text{app}} = \frac{6Q}{WH^2}, \tag{13}$$

where $Q$ is the volumetric flow rate. For non-Newtonian melts, the Schümmer approximation was used to estimate the approximated true wall shear rate or also called Schümmer shear rate $\dot{\gamma}$ [32]:

$$\dot{\gamma} = e\dot{\gamma}_{\text{app}}, \qquad e = \frac{3n}{2n+1}, \tag{14}$$

with $n$ being the power-law index. The corresponding viscosity was then calculated as:

$$\eta = \frac{\tau_W}{\dot{\gamma}} = \frac{WH^3}{12eQ}\frac{\Delta p}{L}\left(1+\frac{H}{W}\right)^{-1}. \tag{15}$$

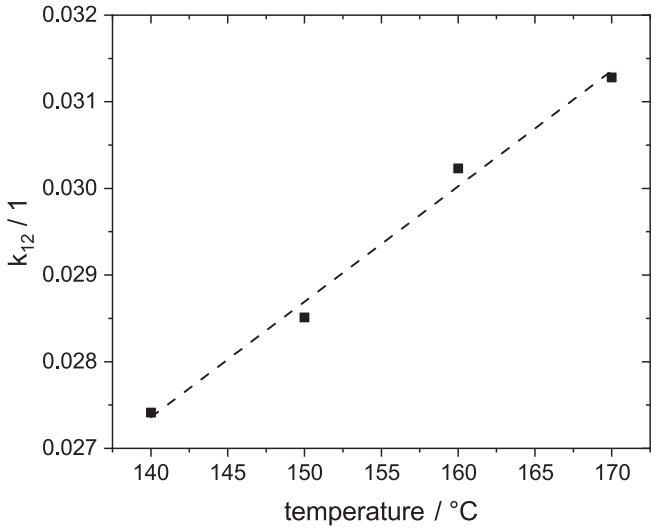


**FIGURE 4** | Temperature dependence of the binary interaction parameter $k_{12}$, fitted using a linear model ($R^2 > 0.99$).

### 2.6 | Design of Experiments

The experimental design was defined to systematically evaluate the influence of shear rate, temperature, and diluent concentration on the viscosity of polymer melts under processing-relevant conditions.

The polymer–diluent combinations listed in Table 1 were investigated. Measurements were performed at two temperatures (200°C and 240°C), with shear rates $\dot{\gamma}$ ranging from 10 to 200 $s^{-1}$. Diluent concentrations were varied from 0% up to approximately 35% by weight, depending on the specific saturation limits and phase stability of the respective polymer–diluent system.

The experimental plan was constructed to probe the operational boundaries of the extrusion system. At high screw speeds, the maximum pressure allowed in the extruder barrel imposed an upper limit on throughput. Conversely, at low polymer throughputs and high diluent concentrations, the injection systems (HPLC pump for liquids, gas dosing station for $CO_2$) were unable to maintain a stable flow. This was caused either by insufficient delivery capacity at high back-pressures or by the extruder failing to convey the resulting low-viscosity melt efficiently toward the die. In such cases, diluent accumulated within the screw channel, leading to unreliable concentration estimates and potentially hazardous operating conditions.

## 3 | Model Development

To capture all different significant effects, we discuss each effect by its own and then combine it to a full model.

### 3.1 | Influence of the Shear Rate

The viscosity of polymer melts exhibits distinct flow regimes. In the present study, the measurable shear rate range was limited to approximately 10–200 $s^{-1}$. Within this range, all polymer–diluent systems exhibited clear shear-thinning behavior with no evidence of a Newtonian plateau. The viscosity is well captured by the power-law model:

$$\eta(\dot{\gamma}) = K\dot{\gamma}^{n-1}, \tag{16}$$

where $K$ is the consistency index and $n$ is the power-law flow index ($n < 1$).

### 3.2 | Temperature Dependence

Since the experimental processing window (200°C–240°C) is located well above the glass transition temperature of polyethylene ($T \gg T_g + 100$ K), the curvature typically described by the WLF equation is negligible. Consequently, we employ the classical Arrhenius equation to determine the horizontal shift factor $a_T$:

$$a_T(T) = \exp\left[\frac{E_a}{R}\left(\frac{1}{T} - \frac{1}{T_{\text{ref}}}\right)\right] \tag{17}$$

where $E_a$ is the flow activation energy, $R$ is the universal gas constant, and $T$ and $T_{\text{ref}}$ are the absolute temperatures.

### 3.3 | Influence of the Pressure

Increasing pressure reduces the specific free-volume in the melt, which limits segmental mobility and results in a noticeable increase in viscosity. This dependency is, particularly, important in high-pressure applications and is frequently represented using an empirical exponential relation proposed by Barus [14–16, 22, 33, 34]:

$$\eta(p) = \eta_{\text{ref}} \exp\left(\beta_p\left(p - p_{\text{ref}}\right)\right), \tag{18}$$

where $\eta_{\text{ref}}$ is the viscosity at the reference pressure $p_{\text{ref}}$, $p$ is the absolute pressure applied, and $\beta_p$ is the pressure sensitivity coefficient.

### 3.4 | Influence of the Diluent Concentration

The reduction in viscosity due to the addition of a diluent is described using two complementary approaches: a phenomenological superposition principle derived from linear viscoelasticity and a thermodynamic prediction based on free-volume theory and equations of state.

#### 3.4.1 | Dual-Shift Viscoelastic Scaling Framework

To rigorously describe the rheological behavior of the diluted polymer melts, we employ the dual-shift framework utilized by Schausberger, Knoglinger, and Janeschitz-Kriegl [8, 11]. This approach is rooted in the method of reduced variables introduced by Ferry [35] and separates the effect of dilution into a structural contribution (vertical shift) and a dynamic contribution (horizontal shift). While the foundational scaling concepts utilized were primarily derived for linear (unbranched)

polymers with narrow molecular weight distributions, this study applies these principles to industrially relevant materials with complex architectures. We explicitly investigate the applicability of these models to systems exhibiting broad and multimodal molecular weight distributions, such as PE-LD and especially PCR.

The vertical shift factor, $b_c$, accounts for the dilution of the entanglement network density. According to molecular theory, the plateau modulus $G_N^0$ scales with the square of the polymer volume fraction $\phi$ (approximated by weight fraction $w_p$) [8, 35–37]:

$$b_c \equiv \frac{G_N^0(\phi)}{G_N^0(1)} \approx w_p^2. \tag{19}$$

The horizontal shift factor, $a_c$, describes the acceleration of relaxation processes. Following Knoglinger et al. [9], the shift is linked to the fractional free volume $f$ via a Doolittle-type equation [11, 38]:

$$\ln a_c \approx B\left(\frac{1}{f_{\text{mix}}} - \frac{1}{f_p}\right). \tag{20}$$

The fractional free volume $f$ is explicitly linked to the number-average molar mass of the mixed system ($M_{n,\text{mix}}$), assuming that additional free volume arises primarily from the increased concentration of chain ends introduced by the diluent [9, 11]:

$$f = f_0 + \frac{A}{M_{n,\text{mix}}}, \quad \text{with} \quad \frac{1}{M_{n,\text{mix}}} = \frac{w_p}{M_{n,p}} + \frac{w_d}{M_{n,d}}. \tag{21}$$

Here, $f_0$ represents the fractional free volume of a polymer chain with infinite molar mass, and $A$ is a specific material parameter. Additionally, a secondary contribution to the horizontal shift arises from the "tube loosening" effect, typically scaling with $w_p^{1.4}$ [11].

#### 3.4.2 | Thermodynamic Prediction Based on Equation of State (EOS)

To predict the shift factors derived in the TCS framework from first principles, we utilize the Sanchez–Lacombe (S-L) EOS. The S-L EOS is applied to the virgin polymer-solvent mixture to calculate the density of the mixture ($V_m$) as a function of diluent concentration, temperature, and pressure.

These density data are linked to viscosity using a modified Kelley–Bueche equation, as proposed by Gerhardt and Kwag [12, 18]. This formulation describes the concentration shift factor $a_c$:

$$a_c = (1-w_d)^n \left(\frac{V_p}{V_m}\right)^n \exp\left(\frac{1}{f_m} - \frac{1}{f_p}\right), \tag{22}$$

where $n$ is the iso-free-volume viscosity scaling exponent (typically 3.0–3.5 for entangled systems [5, 12, 39]). The fractional free-volume $f$ is physically defined as:

$$f = \frac{V - V^0}{V}, \tag{23}$$

where $V$ is the specific volume at the current state and $V^0$ is the specific occupied volume determined from shear-rate dependent viscosity data of the pure polymer [5]:

$$\eta = B \exp\left(\frac{V}{V - V^0}\right). \tag{24}$$

## 4 | Results and Discussion

Our comprehensive rheological characterization of polymer-diluent systems under industrial processing conditions revealed several key insights into the mechanisms that govern viscosity reduction. This section presents the systematic evaluation of various model formulations and their ability to predict the complex interdependencies between shear rate, temperature, pressure, and diluent concentration effects.

### 4.1 | Validation of No-Slip Condition

Prior to the main investigation, the potential occurrence of wall slip was assessed to ensure the validity of the rheological data. To verify the no-slip condition, frequency sweeps were performed using a parallel-plate rheometer at different gap heights ($h_1 = 1$ mm and $h_2 = 0.5$ mm) and high diluent concentrations, following the method proposed by Yoshimura and Prud'homme [40].

Typically, wall slip manifests as a gap-dependent reduction in apparent viscosity. However, the experimental data revealed no significant reduction in viscosity at the reduced gap height. Consequently, wall slip effects are considered negligible for the investigated regime.

### 4.2 | Validation of Thermorheological Simplicity

The applicability of the Time–Temperature Superposition (TTS) principle to the PE-LD PCR was assessed, as recyclates may exhibit thermorheological complexity due to compositional heterogeneity or branching. Van Gurp–Palmen (vGP) plots derived from small amplitude oscillatory shear (SAOS) measurements demonstrated excellent data collapse without the need for vertical shifting ($b_T$), as shown in Figure 5. This confirms thermorheological simplicity within the investigated experimental window [41].

Furthermore, the flow activation energy determined via in-line slit rheometry ($E_a \approx 3.5 \times 10^4$ J/mol) shows reasonable agreement with offline SAOS measurements ($E_a \approx 3.0 \times 10^4$ J/mol). The observed deviation of approximately 15% ($E_{a,\text{slit}} > E_{a,\text{SAOS}}$) is primarily attributed to the simplifying assumptions in the slit flow analysis presented in Section 2.5. While the evaluation assumes a linear pressure gradient, implicitly neglecting the pressure dependence of viscosity to facilitate analytical solution, the physical melt viscosity remains subject to the Barus effect. Since the extrusion pressure naturally increases with decreasing temperature, pressure-induced viscosity variations are

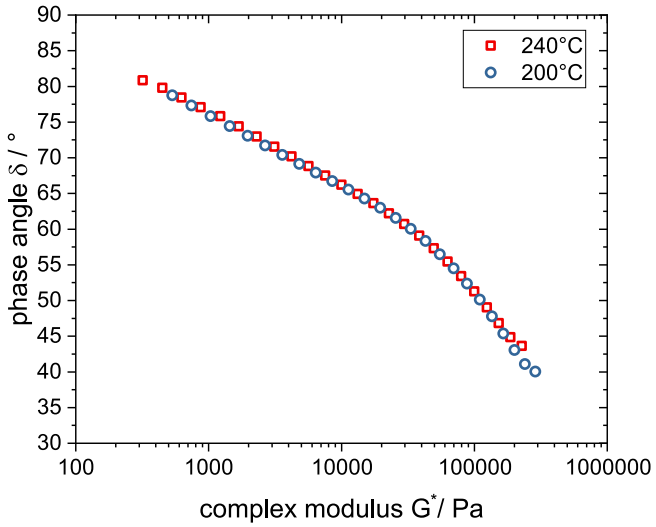


**FIGURE 5** | Van Gurp–Palmen plot for PE-LD PCR derived from SAOS frequency sweeps (triplicates) at 200°C and 240°C via parallel plate rheometry. The distinct data collapse of the isotherms confirms thermorheological simplicity within the experimental window.

superimposed onto the temperature sensitivity. This effectively inflates the apparent flow activation energy in the slit measurements compared to the ambient-pressure SAOS data. Minor remaining discrepancies may be ascribed to the inherent differences in sensitivity between the two methods.

### 4.3 | Model Selection and Validation Strategy

To identify the optimal constitutive model for polymer–diluent systems, semiempirical, free-volume based but still empirically fitted and pure theoretical formulations were systematically evaluated against the experimental data. The selection process was guided by three primary criteria: (i) statistical accuracy, quantified by the coefficient of determination ($R^2$), and mean relative error (MRE); (ii) physical consistency of the fitted parameters across different material systems; and (iii) practical applicability in industrial environments, explicitly considering the accessibility of required thermodynamic data.

Consistent with the methodology established in our preceding work [23], a power-law model combined with an Arrhenius-type temperature term served as the baseline framework. These components have proven robust for describing shear-thinning behavior and thermal sensitivity within the experimental window investigated ($\dot{\gamma} = 10$ to 200 $s^{-1}$, $T = 200^{\circ}C$–$240^{\circ}C$).

### 4.4 | Pressure Dependence: Experimental Validation and Theoretical Implications

Investigation of pressure-dependent rheological behavior revealed important insights into the fundamental limitations of slit-die rheometry for polymer–diluent systems. Wall normal stress measurements along the slit die exhibited an almost perfectly linear profile $T_{yy}(b,z)$, where $b$ is half the slit height and $z$ the flow direction. This linear relationship indicates a constant pressure gradient and confirms the absence of significant viscous shear heating under the operating conditions investigated.

However, as demonstrated by Han et al. [31], the fundamental challenge in extracting true hydrostatic pressure effects from slit-die measurements lies in the coupled nature of pressure and deviatoric stress contributions. The measured wall normal stress is given by:

$$T_{yy}(b,z) = -p(b,z) + \sigma_{yy}(b), \tag{25}$$

where $p(b,z)$ represents the hydrostatic pressure and $\sigma_{yy}(b)$ the deviatoric stress component at the wall. Since both $T_{yy}(b,z)$ and $p(b,z)$ vary with the flow coordinate $z$, separating pressure and deviatoric contributions becomes impossible in the fully developed flow region.

The strict linearity of the $T_{yy}$ profiles observed (characterized by $\partial T_{yy}/\partial z = \text{constant}$) justifies the omission of pressure-induced viscosity variations, as the constant pressure gradient ensures that pressure effects remain uniform throughout the measurement domain. This finding contradicts earlier claims by Royer et al. [13] regarding the significance of pressure effects in similar experimental configurations and supports the omission of pressure terms in our constitutive model.

### 4.5 | Concentration Dependence: Comparison of Modeling Strategies

Modeling the effect of diluent concentration necessitates balancing predictive accuracy against parameter availability. We evaluated three distinct strategies. For the first two, viscosity reduction is decoupled into frictional ($a_c$) and structural ($b_c$) contributions. The vertical shift factor $b_c$, representing the dilution of the entanglement network, is fixed to the theoretical scaling $b_c = w_p^2$, where $w_p = (1 - w_d)$. The models differ in their derivation of $a_c$:

1. *Semiempirical model*: Designed for robust process control, combining entanglement dilution ($b_c$) with a simplified exponential friction term. The horizontal shift is governed by a single fitted sensitivity coefficient $\beta_c$:

$$a_c(w_d) = \exp(-\beta_c w_d); \quad b_c = w_p^2. \tag{26}$$

2. *Schausberger model*: A framework describing the horizontal shift by superimposing free-volume-induced friction reduction with a topological "tube loosening" effect and a fitted empirical factor $A$ [8]:

$$a_c(w_d) = (1-w_d)^{1.4} \exp\left(\frac{B}{f_0 + A/M_{n,\text{mix}}} - \frac{B}{f_0 + A/M_{n,p}}\right); \quad b_c = w_p^2. \tag{27}$$

3. *Kelley–Bueche EOS model*: A predictive approach based on first principles using the S-L EOS [12]. This formulation yields a unified viscosity reduction factor without an explicit $b_c$:

$$a_c(w_d) = (1 - w_d)^n \left(\frac{V_p}{V_m}\right)^n \exp\left(\frac{1}{f_m} - \frac{1}{f_p}\right). \quad (28)$$

### 4.6 | Master Curve Construction and Global Superposition

To consolidate the rheological data measured across varying shear rates, temperatures, and diluent concentrations, a unified superposition principle was applied. This approach combines the well-established TTS with TCS, allowing all experimental data points to be shifted onto a single reference master curve representing the behavior of the neat polymer at the reference temperature ($T_{ref} = 200^{\circ}C$) and reference diluent concentration ($w_d = 0$ %).

The shifting procedure accounts for the variations in relaxation times and plateau modulus induced by temperature and dilution. Consequently, the reference viscosity $\eta_{ref}$ and reference shear rate $\dot{\gamma}_{ref}$ are calculated from the measured quantities as:

$$\eta_{ref}(\dot{\gamma}_{ref}) = \frac{\eta_{meas}(\dot{\gamma}_{meas}, T, w_d)}{a_T(T) a_c(w_d) b_c(w_d)} \quad (29)$$

$$\dot{\gamma}_{ref} = \dot{\gamma}_{meas} a_T(T) a_c(w_d) \quad (30)$$

Figure 6 displays the resulting superposition. Figure 6a,b utilize the shift factors derived from the semiempirical model. The excellent data collapse observed for both the virgin PE-HD and the post-consumer recyclate (PE-LD PCR) confirms that this robust model successfully captures the combined effects of temperature and diluent concentration. Figure 6c illustrates the superposition for PE-HD using the physically rigorous Schausberger model, yielding an equally smooth master curve and validating the distinct separation of frictional ($a_c$) and structural ($b_c$) contributions.

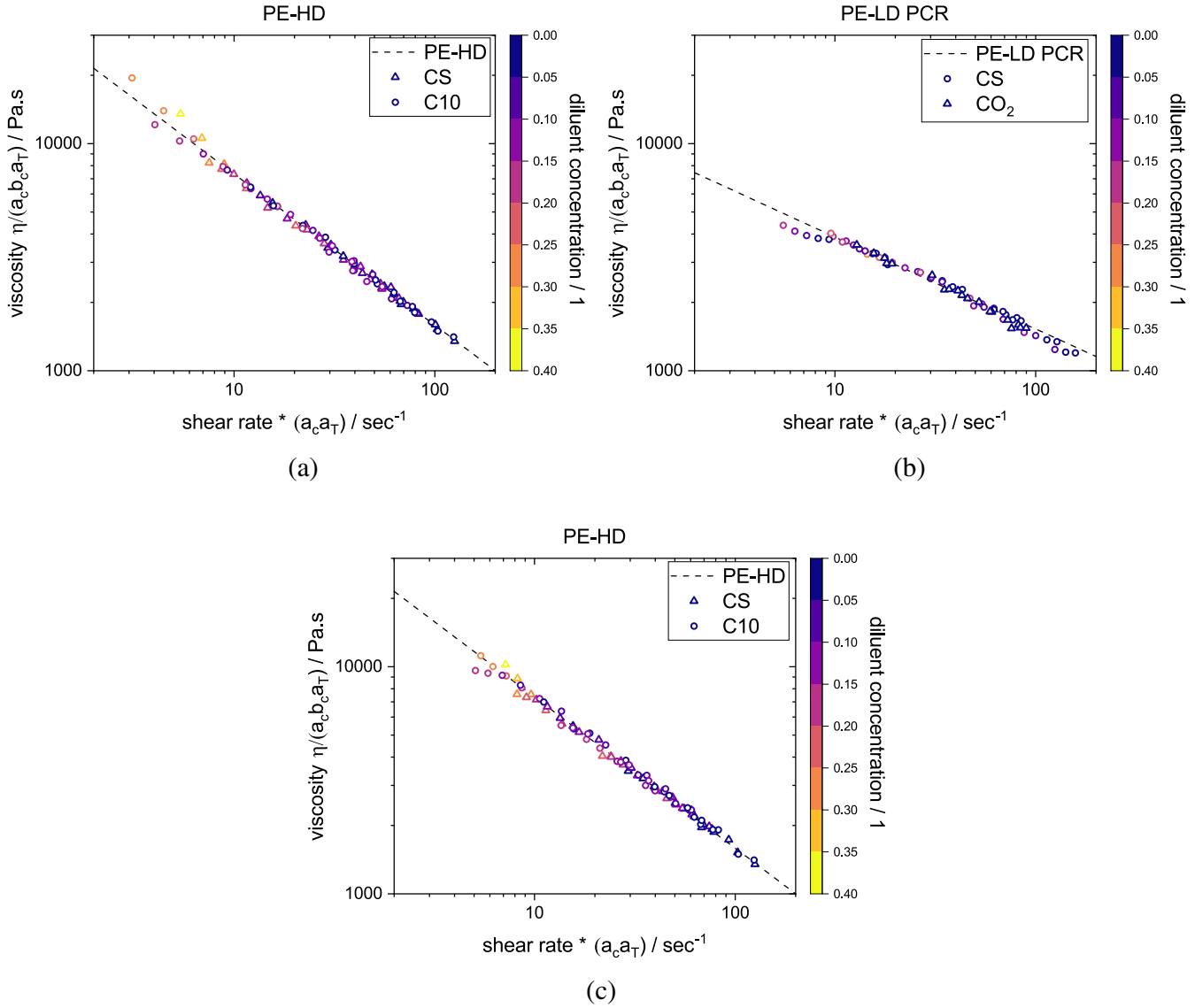


**FIGURE 6** | Unified master curves generated by shifting viscosity data onto the reference state of the neat polymer at 200°C [cite: 3]. (a, b) Superposition achieved using the robust semiempirical model for PE-HD and PE-LD PCR, respectively. (c) Superposition for PE-HD based on the molecular-weight-dependent Schausberger model. Note that the Schausberger framework was excluded for the PCR grade due to the unavailability of molecular mass distribution data.

**TABLE 2** | Optimized fitting parameters and statistical evaluation.

| | | | | | | Semiempirical model | | | Schausberger model | | | | |
|---|---|---|---|---|---|---|---|---|---|---|---|---|---|
| Polymer | Diluent | $T$ (°C) | $K$ (Pas) | $n$ | $E_a$ (J mol$^{-1}$) | $\beta_c$ | $MRE$ | $R^2$ | $A$ (g mol$^{-1}$) | $B$ | $f_0$ | $MRE$ | $R^2$ |
| PE-HD | C10 | 200 | 34,070 | 0.334 | 3.18E4 | 6.57 | 3.96% | 0.974 | 448 | 1.00 | 0.305 | 2.8% | 0.965 |
| PE-HD | C10 | 240 | | | | 4.78 | 1.97% | 0.976 | 181 | 1.0 | 0.322 | 2.2% | 0.972 |
| PE-HD | BM | 200 | | | | 9.58 | 4.25% | 0.965 | 201 | 1.0 | 0.305 | 2.9% | 0.966 |
| PE-HD | BM | 240 | | | | 9.32 | 2.36% | 0.986 | 181 | 1.0 | 0.322 | 4.2% | 0.964 |
| PE-LD PCR | BM | 200 | 9852 | 0.595 | 3.50E4 | 4.50 | 3.19% | 0.965 | | | | | |
| PE-LD PCR | BM | 240 | | | | 4.03 | 4.29% | 0.924 | | | | | |
| PE-LD PCR | CO2 | 200 | | | | 16.51 | 2.89% | 0.880 | | | | | |
| PE-LD PCR | CO2 | 240 | | | | 11.47 | 2.98% | 0.805 | | | | | |

**TABLE 3** | Characteristic S-L parameters obtained from different sources.

| Material | $T^*$ (K) | $P^*$ (MPa) | $\rho^*$ (kg m$^{-3}$) | Source |
|---|---|---|---|---|
| PE-HD | 640 | 388.8 | 890 | Park et al. [14] |
| PE-LD | 682.8 | 411.9 | 884.2 | Ginting et al. [29] |
| *n*-decane | 530 | 305 | 837 | Sanchez et al. [17] |
| $CO_2$ | 319 | 727.4 | 1725 | Park et al. [14] |

## 4.7 | Quantitative Evaluation of Model Performance

Table 2 summarizes the fitting parameters based on the fitting metrics, which can be found in the appendix. Despite its simplicity, the semiempirical model provides a remarkably good description across all systems ($R^2 > 0.96$). The sensitivity coefficient $\beta_c$ effectively captures the varying plasticization efficiency; for example, the specialty solvent requires a higher coefficient ($\beta_c \approx 9.6$) compared to *n*-decane ($\beta_c \approx 6.6$) at 200°C.

This accuracy is attributed to the investigated concentration range (0%–35%). In this regime, the strong nonlinear curvature of Doolittle-type functions is not fully pronounced, allowing the exponential approximation to suffice. For PE-HD systems where molecular data was available, the Schausberger model yields the highest precision (MRE 2.2%–2.9%). The fitted free volume fraction $f_0$ (0.30–0.32) aligns with theoretical expectations for polyethylene melts.

## 4.8 | Physics-Based Analysis Using the S-L EOS

To understand the thermodynamic basis of the observed viscosity reduction, the S-L EOS framework was implemented using parameters from Sanchez and Ginting [17, 29] as shown in Table 3.

### 4.8.1 | Theoretical Predictions Versus Experimental Reality

Using the S-L EOS framework, mixture densities were calculated as functions of diluent concentration, temperature, and pressure. These density predictions were subsequently converted to concentration shift factors $a_c$ using the modified Kelley–Bueche relation, enabling a direct comparison with experimental measurements for both the PE-HD/*n*-decane and the PE-LD PCR/$CO_2$ systems (Figure 7).

In order to validate the theoretical free-volume predictions against the rheological measurements, it is necessary to separate the individual mechanisms contributing to the viscosity reduction. According to the framework established by Schausberger et al. [8, 9], the total reduction arises from two concurrent effects: the decrease in monomeric friction coefficient, represented by the horizontal shift factor $a_c$, and the dilution of the entanglement network density, represented by the vertical shift factor $b_c$. As the Kelley–Bueche model is strictly limited to the frictional component dependent on free volume, the experimental zero-shear viscosities, as well as the Schausberger model predictions for PE-HD, were scaled by the theoretical entanglement dilution factor. By factoring out the entanglement contribution (assuming $b_c = w_p^2$), the data presented in Figure 7 allow for an isolated assessment of the friction reduction capabilities of the diluent.

Despite this scaling, a distinct quantitative discrepancy is evident in both systems. While the theoretical framework captures the qualitative exponential trend, the KB model coupled with S-L EOS

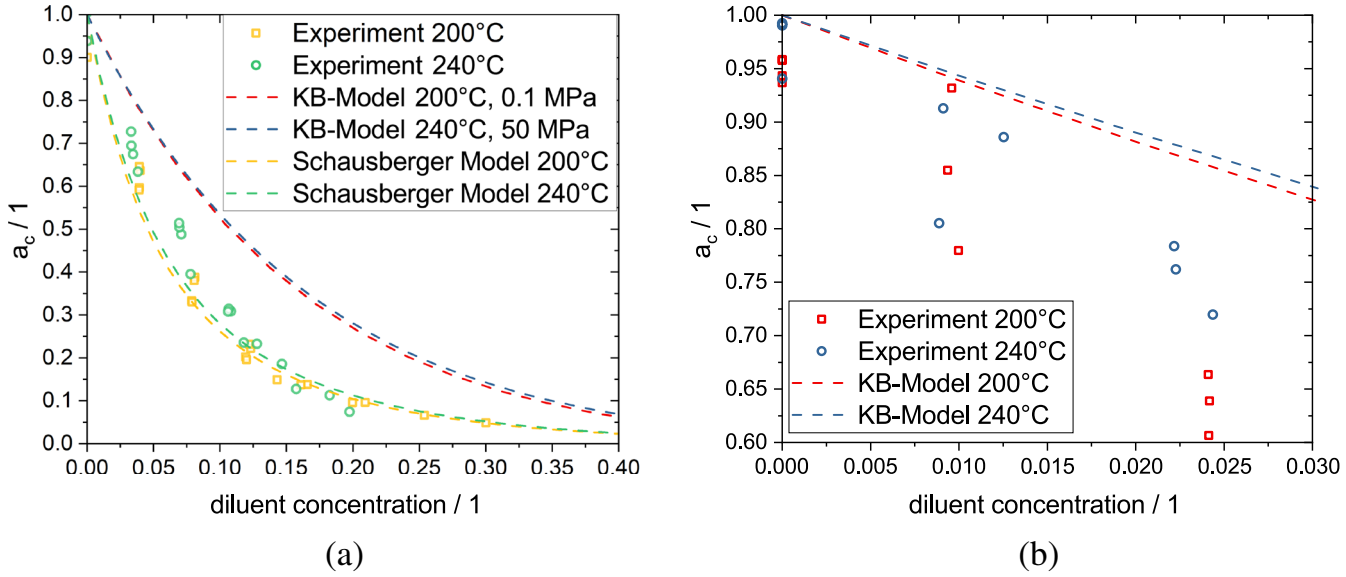


**FIGURE 7** | Comparison of concentration shift factors $a_c$ for (a) PE-HD/C10 and (b) PE-LD PCR/$CO_2$. The Kelley–Bueche (KB) model predictions (derived from S-L EOS) are compared with experimental results. (a) Additionally includes the Schausberger model, which was omitted for (b) due to missing molecular data. In both panels, experimental data points were scaled by the entanglement dilution factor $b_c$ to isolate monomeric friction effects. Despite this correction, the KB model consistently underestimates the viscosity reduction in both systems, predicting notably higher $a_c$ values than observed experimentally.

significantly underestimates the extent of viscosity reduction (i.e., it predicts higher $a_c$ values than observed).

For the PE-HD/C10 system (Figure 7a), this deviation highlights that the fractional free volume derived from equilibrium thermodynamics (EOS) yields a more modest reduction in monomeric friction than the transport-relevant free volume operative in the real melt.

Of particular interest is the PE-LD PCR/$CO_2$ system (Figure 7b). Although the combination of S-L EOS and KB theory is frequently applied in literature to model $CO_2$-plasticized polymers, our results indicate that the model underestimates the plasticization efficiency even for this supercritical diluent. A critical factor contributing to this underestimation is the specific application domain of the KB model. Historically, this framework has been primarily applied to amorphous polymers processed in the vicinity of their glass transition temperature ($T_g$). Under those conditions, the neat polymer possesses a significantly lower fractional free volume, meaning that the infusion of a high-free-volume diluent like $CO_2$ induces a massive relative increase in available volume. In contrast, the polyethylene systems investigated here are processed far above their glass transition ($T \gg T_g + 100$ K). Consequently, the polymer matrix already exhibits a high intrinsic fractional free volume. In this regime, the standard KB approach predicts a less dramatic relative gain in free volume, thereby possibly underestimating the sharp drop in friction observed experimentally.

#### 4.8.2 | Implications for Model Development

The physics-based analysis using the S-L EOS served multiple purposes. First, it provided a physical rationale for the exponential concentration dependence employed in the empirical model. While the magnitude of the reduction was underestimated by the pure free-volume approach, the analysis confirms that the functional form used in the Schausberger model is consistent with fundamental thermodynamic principles governing free volume changes.

Second, the EOS analysis offered theoretical insight into the temperature sensitivity. It supports the observation that within the investigated processing range, concentration shift factors exhibit weak temperature dependence, justifying the use of a temperature-independent simplification in our empirical modeling.

Finally, the S-L EOS framework establishes a theoretical foundation for future model development. Although direct quantitative prediction remains challenging, the framework successfully captures qualitative trends. This offers potential for hybrid modeling approaches, where fundamental material properties define the scaling behavior, while minimal experimental data points calibrate the magnitude of the plasticization effect.

### 4.9 | Final Model Formulation for Industrial Application

Based on the trade-off between model complexity, data availability, and predictive performance, we identify the semiempirical exponential model as the optimal constitutive equation for process simulation in this context. It balances the need for robust handling of recycling materials (where molecular data is often missing) with sufficient accuracy for process control. The final constitutive equation is given by:

$$\eta(\dot{\gamma}, T, c) = K\dot{\gamma}^{n-1} \exp\left[\frac{E_a}{R}\left(\frac{1}{T} - \frac{1}{T_{\text{ref}}}\right)\right] \exp\left(-\beta_c c\right). \tag{31}$$

The predictive capability of this formulation is visualized in the global scatter plot in Figure 8a. The model achieves excellent agreement across the full parameter space for all investigated systems, including the postconsumer recyclates (PE-LD PCR) and supercritical $CO_2$, with the vast majority of data points falling within the $\pm 10$ % error margins.

For comparison, Figure 8b displays the performance of the physically more rigorous Schausberger model. While this model yields slightly higher precision and a tighter scatter for the virgin PE-HD systems, its application was restricted to materials with known molecular weight distributions. Consequently, it could not be applied to the PCR grades.

## 5 | Conclusion

In this study, we established a comprehensive rheological framework that bridges the gap between fundamental thermodynamic principles and practical process modeling for diluted polyethylene melts. By investigating four distinct polymer–diluent systems, including virgin PE-HD and recycled PE-LD (PCR) with diluents ranging from *n*-decane, a specially developed diluent for the CreaSolv-technology and to supercritical $CO_2$. We derived a robust constitutive model capable of predicting viscosity reduction under industrial processing conditions.

A critical prerequisite for this modeling effort was the exclusion of rheological artifacts. Given the lubricating nature of short-chain alkanes, particular attention was paid to wall slip. Parallel-plate rheometry with varying gap heights confirmed the absence of slip in the investigated shear rate regime ($\dot{\gamma} = 10 - 200\ s^{-1}$), ensuring that the observed viscosity reductions were purely bulk material responses.

The modeling strategy was evaluated across three levels of physical depth, yielding the following key insights:

- *Industrial robustness*: The proposed four-parameter semiempirical model (Equation 31) proved to be the most effective tool for practical application. It achieved excellent statistical accuracy ($MRE < 5$ %, $R^2 > 0.96$ (for C10 and CS) and $R^2 > 0.8$ for $CO_2$) without requiring complex molecular weight data. This makes it, particularly, valuable for describing PCR grades where feedstock variability prevents detailed molecular characterization.
- *Physical precision*: When molecular mass distribution data is available, the Schausberger model offers superior physical fidelity. It captures the curvature of the shift factor $a_c$ at higher concentrations, a feature that simple exponential models approximate linearly. However, its dependence on the empirically determined parameter $A$ and molecular weight data limits its immediate applicability to well-characterized virgin materials.
- *Thermodynamic fundamentals*: The application of the S-L EOS coupled with the Kelley–Bueche framework provided a theoretical benchmark. While it successfully validated the exponential functional form of the dilution effect, it quantitatively underestimated the magnitude of viscosity reduction. This discrepancy suggests that for semicrystalline polymers which are commonly processed far above their glass transition temperature ($T \gg T_g$), the standard free-volume additivity assumes a "stiffer" system than reality presents. The specific friction-reducing effect of low-molecular-weight diluents appears to exceed the predictions derived solely from equilibrium hole free volume, highlighting a need for refined transport theories in this regime.

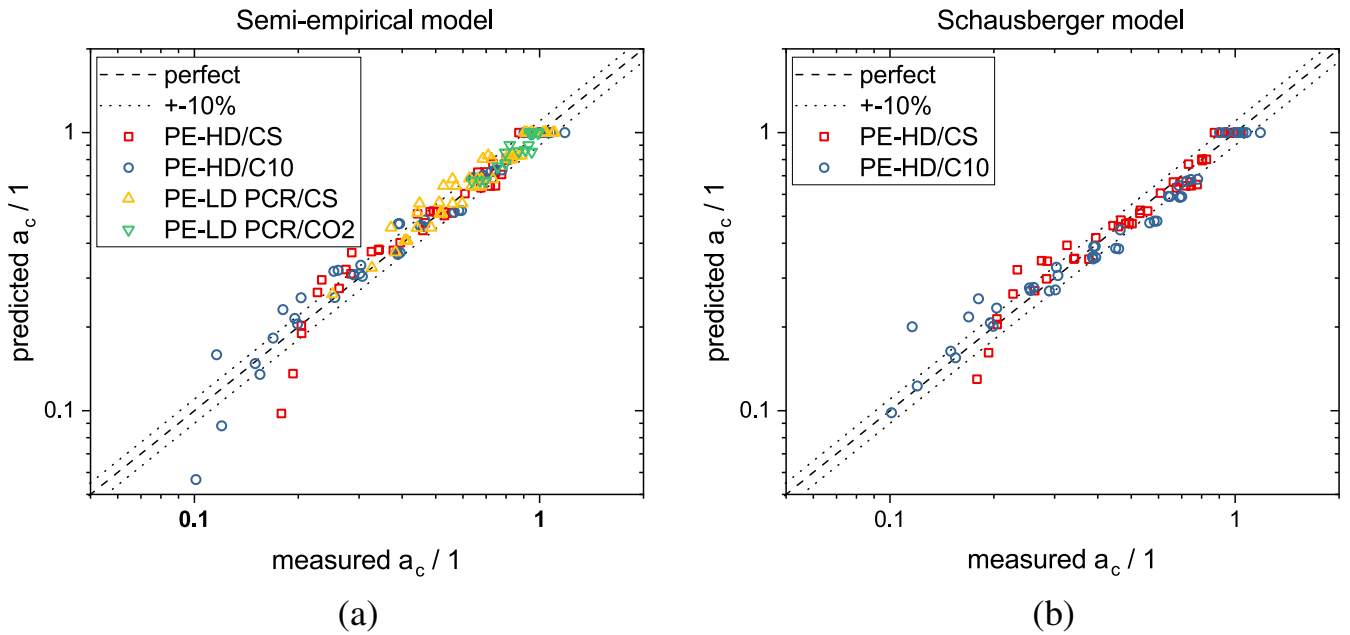


**FIGURE 8** | Global assessment of predictive accuracy comparing measured vs. predicted $a_c$. (a) Predictions using the final semiempirical model (Equation 31) covering all investigated polymer–diluent systems including PCR. (b) Predictions using the Schausberger model, restricted to PE-HD systems where molecular mass distribution data was available. The dashed diagonal represents the line of perfect agreement and the dotted lines are the 10% deviation of the perfect fit.

Looking forward, future research should focus on extending the experimental window to higher diluent concentrations to empirically verify the curvature predicted by the Schausberger model. Additionally, while parallel-plate tests ruled out slip here, extrusion experiments with varying slit heights are recommended to validate these findings under continuous flow conditions.

Ultimately, this work provides a ready-to-use computational framework for the polymer industry. By enabling the accurate prediction of rheological behavior for diluent-loaded melts without extensive material characterization, the developed model facilitates the integration of rheology into digital twins. This is a crucial step toward real-time process optimization in advanced processing technologies.

### Author Contributions

**Ernst Georg Viehböck:** conceptualization, investigation, writing – original draft, methodology, validation, visualization, writing – review and editing, software, formal analysis, data curation. **Alexander Hammer:** conceptualization, investigation, methodology, writing – review and editing, formal analysis, validation, supervision. **Markus Kirchmayr:** resources. **Christof Murnig:** resources. **Christian Paulik:** writing – review and editing, conceptualization, project administration, resources, supervision, funding acquisition. **Gerald Berger-Weber:** conceptualization, funding acquisition, writing – review and editing, project administration, supervision, resources.


### Acknowledgments

During the preparation of this work, the authors used Chat GPT-5 and Google Gemini in order to increase readability. After using this tool, the authors reviewed and edited the content as needed and employed a professional editor and took full responsibility for the content of the published article. Open Access funding provided by Johannes Kepler Universitat Linz/KEMÖ.

### Funding

The authors acknowledge support through the FTI initiative circular economy "circPLAST-mr," funded by the BMIMI (Federal ministry of Innovation, Mobility, and Infrastructure of the Republic of Austria) and the FFG (Austrian Research Promotion Agency)—funding number 889843. This work was conducted as part of the COMET Center CHASE, funded within the COMET—Competence Centers for Excellent Technologies program by the BMIMI, the BMWET, and the Federal Provinces of Upper Austria and Vienna. The COMET program is managed by the FFG. Supported by Johannes Kepler Open Access Publishing Fund and the federal state Upper Austria.


### Data Availability Statement

The data that support the findings of this study are available from the corresponding author upon reasonable request.

### References


1. T. A. Osswald, *Understanding Polymer Processing: Processes and Governing Equations*, 2nd ed. (Carl Hanser Verlag GmbH & Co. KG, 2017).

2. W. Michaeli, *Plastics Processing: An Introduction* (Hanser, 1995).

3. S.-T. Lee and C. B. Park, eds., *Foam Extrusion: Principles and Practice. Polymeric Foams Series*, 2nd ed. (CRC Press, 2014).

4. K. V. Pochivalov, T. N. Lebedeva, A. N. Ilyasova, A. V. Basko, and Y. V. Kudryavtsev, "A New Look at the Semicrystalline Polymer – Liquid Systems: Phase Diagrams Low-Density Polyethylene—n-Alkanes," *Fluid Phase Equilibria* 471 (2018): 1–7.

5. F. N. Kelley and F. Bueche, "Viscosity and Glass Temperature Relations for Polymer-Diluent Systems," *Journal of Polymer Science* 50 (1961): 549–556.

6. H. Fujita and A. Kishimoto, "Diffusion-Controlled Stress Relaxation in Polymers. II. Stress Relaxation in Swollen Polymers," *Journal of Polymer Science* 28 (1958): 547–567.

7. H. Fujita and E. Maekawa, "Viscosity Behavior of the System Polymethyl Acrylate and Diethyl Phthalate Over the Complete Range of Composition," *Journal of Physical Chemistry* 66 (1962): 1053–1058.

8. A. Schausberger, H. Knoglinger, and H. Janeschitz-Kriegl, "The Role of Short Chain Molecules for the Rheology of Polystyrene Melts. II. Linear Viscoelastic Properties," *Rheologica Acta* 26 (1987): 468–473.

9. H. Knoglinger, A. Schausberger, and H. Janeschitz-Krieg, "The Role of Short Chain Molecules for the Rheology of Polystyrene Melts. I. Molar Mass Dependent Shift Factors," *Rheologica Acta* 26 (1987): 460–467.

10. E. Kastner, "Zeit-Konzentration-Superposition am Beispiel konzentrierter Polyethylenlösungen," 1996.

11. A. Schausberger and I. V. Ahrer, "On the Time-Concentration Superposition of the Linear Viscoelastic Properties of Plasticized Polystyrene Melts Using the Free Volume Concept," *Macromolecular Chemistry and Physics* 196 (1995): 2161–2172.

12. L. J. Gerhardt, A. Garg, C. W. Manke, and E. Gulari, "Concentration-Dependent Viscoelastic Scaling Models for Polydimethysiloxane Melts With Dissolved Carbon Dioxide," *Journal of Polymer Science Part B: Polymer Physics* 36 (1998): 1911–1918.

13. J. R. Royer, Y. J. Gay, J. M. Desimone, and S. A. Khan, "High-Pressure Rheology of Polystyrene Melts Plasticized With CO2: Experimental Measurement and Predictive Scaling Relationships," *Journal of Polymer Science Part B: Polymer Physics* 38 (2000): 3168–3180.

14. H. E. Park and J. M. Dealy, "Effects of Pressure and Supercritical Fluids on the Viscosity of Polyethylene," *Macromolecules* 39 (2006): 5438–5452.

15. H. E. Park, J. M. Dealy, A. Co, G. L. Leal, R. H. Colby, and A. J. Giacomin, "Effects of Supercritical Fluids, Pressure, Temperature, and Molecular Structure on the Rheological Properties of Molten Polymers," *AIP Conference Proceedings* 1027 (2008): 366–368.

16. T. Schaible and C. Bonten, "In-Line Measurement and Modeling of Temperature, Pressure, and Blowing Agent Dependent Viscosity of Polymer Melts," *Applied Rheology* 32 (2022): 69–82.

17. I. C. Sanchez and R. H. Lacombe, "Statistical Thermodynamics of Polymer Solutions," *Macromolecules* 11 (1978): 1145–1156.

18. C. Kwag, "Rheology of Molten Polystyrene With Dissolved Gases" (PhD thesis, Wayne State, 1998).

19. S. Areerat, T. Nagata, and M. Ohshima, "Measurement and Prediction of LDPE/$CO_2$ Solution Viscosity," *Polymer Engineering & Science* 42 (2002): 2234–2245.

20. C.-Y. Ma and C. Dae Han, "Measurement of the Viscosities of Mixtures of Thermoplastic Resin and Fluorocarbon Blowing Agent," *Journal of Cellular Plastics* 18 (1982): 361–370.

21. M. Lee, "Measurements and Modeling of PS/Supercritical CO2 Solution Viscosities," *Polymer Engineering & Science* 39 (1999): 99–109.

22. X. Qin, M. Thompson, A. Hrymak, and A. Torres, "Rheology Studies of Polyethylene/Chemical Blowing Agent Solutions Within an Injection Molding Machine," *Polymer Engineering and Science* 45 (2005): 1108–1118.

23. E. G. Viehböck, A. Hammer, M. Kirchmayr, C. Murnig, C. Paulik, and G. Berger-Weber, "Slitrheometry-Based Characterization of the Flow Behavior of Diluted Polymer Melts," *Journal of Rheology* 70 (2026): 35–45.

24. S. Wagner, G. Kronberger, A. Beham, et al., "Architecture and Design of the HeuristicLab Optimization Environment," in *Advanced Methods and Applications in Computational Intelligence, Topics in Intelligent Engineering and Informatics*, vol. 6, ed. R. Klempous, J. Nikodem, W. Jacak, and Z. Chaczko (Springer International Publishing, 2014), 197–261.

25. C. Marschik, M. Dörner, W. Roland, J. Miethlinger, V. Schöppner, and G. Steinbichler, "Application of Network Analysis to Flow Systems With Alternating Wave Channels: Part A (Pressure Flows)," *Polymers* 11 (2019): 1488, https://doi.org/10.3390/polym11091488.

26. A. Hammer, W. Roland, M. Zacher, S. Kohl, and G. Berger–Weber, "Experimental Validation of Non–Newtonian Stratified Co–Extrusion Prediction Models Using a Digital Process Twin," *Polymer Engineering and Science* 62 (2022): 3902–3922.

27. A. Garg, E. Gulari, and C. W. Manke, "Thermodynamics of Polymer Melts Swollen With Supercritical Gases," *Macromolecules* 27 (1994): 5643–5653.

28. R. A. Orwoll and J. A. Small, "Volume Changes of Mixing and Excess Coefficients of Thermal Expansion for Solutions of Polymethylene in n-Decane," *Macromolecules* 6 (1973): 755–757.

29. R. R. Ginting, I. Ushiki, and K. Otsubo, "CO2 Solubilities in Low-Density Polyethylene (LDPE) in Its Molten State Over High Temperatures and Pressures Conditions," *Journal of CO2 Utilization* 99 (2025): 103164.

30. W. Michaeli and C. Hopmann, *Extrusion Dies for Plastics and Rubber*, 4th ed. (Hanser Publishers, 2016).

31. C. D. Han, *Rheology and Processing of Polymeric Materials* (Oxford University Press, 2007).

32. P. Schümmer and R. H. Worthoff, "An Elementary Method for the Evaluation of a Flow Curve," *Chemical Engineering Science* 33 (1978): 759–763.

33. C. Barus, "Isothermals, Isopiestics and Isometrics Relative to Viscosity," *American Journal of Science* s3-45 (1893): 87–96.

34. J. M. Dealy and J. Wang, *Melt Rheology and Its Applications in the Plastics Industry. Engineering Materials and Processes* (Springer Netherlands, 2013).

35. J. D. Ferry, *Viscoelastic Properties of Polymers* (John Wiley & Sons, 1980).

36. W. Graessley, "Polymer Chain Dimensions and the Dependence of Viscoelastic Properties on Concentration, Molecular Weight and Solvent Power," *Polymer* 21 (1980): 258–262.

37. R. H. Colby, L. J. Fetters, W. G. Funk, and W. W. Graessley, "Effects of Concentration and Thermodynamic Interaction on the Viscoelastic Properties of Polymer Solutions," *Macromolecules* 24 (1991): 3873–3882.

38. A. K. Doolittle, "Studies in Newtonian Flow. II. The Dependence of the Viscosity of Liquids on Free-Space," *Journal of Applied Physics* 22, no. 12 (1951): 1471–1475, https://doi.org/10.1063/1.1699894.

39. D. W. van Krevelen and K. te Nijenhuis, *Properties of Polymers: Their Correlation With Chemical Structure: Their Numerical Estimation and Prediction From Additive Group Contributions*, 4th ed. (Elsevier, 2009).

40. A. Yoshimura and R. K. Prud'homme, "Wall Slip Corrections for Couette and Parallel Disk Viscometers," *Journal of Rheology* 32 (1988): 53–67.

41. M. van Gurp and J. Palmen, "Time-Temperature Superposition for Polymeric Blends," *Rheology Bulletin* 67 (1998): 5–8.

## Appendix A

### Fitting Metrics

In order to fit all models evaluated using consistent performance criteria, several key metrics were defined and applied. The used fitting parameter is the weighted quadratic error *WQE*:

$$WQE = \sum_{i=1}^{n} \frac{(x_i - y_i)^2}{x_i}, \tag{A1}$$

where $x_i$ is the measured value, $y_i$ is the predicted value, and $n$ is the total number of data points.

Additionally, the coefficient of determination $R^2$ was calculated to assess how well the model explains the variance in the experimental data:

$$R^2 = 1 - \frac{\sum_{i=1}^{n} (x_i - y_i)^2}{\sum_{i=1}^{n} (x_i - \bar{x})^2}, \tag{A2}$$

where $\bar{x}$ is the mean of the measured values.

Finally, the mean relative error *MRE* was determined as:

$$MRE = \frac{1}{n} \sum_{i=1}^{n} \left| \frac{x_i - y_i}{x_i} \right|. \tag{A3}$$

In all fitting tasks, the primary objective was to minimize the weighted quadratic error *WQE*, while the additional metrics $R^2$ and *MRE* were used solely for comparative performance assessment.

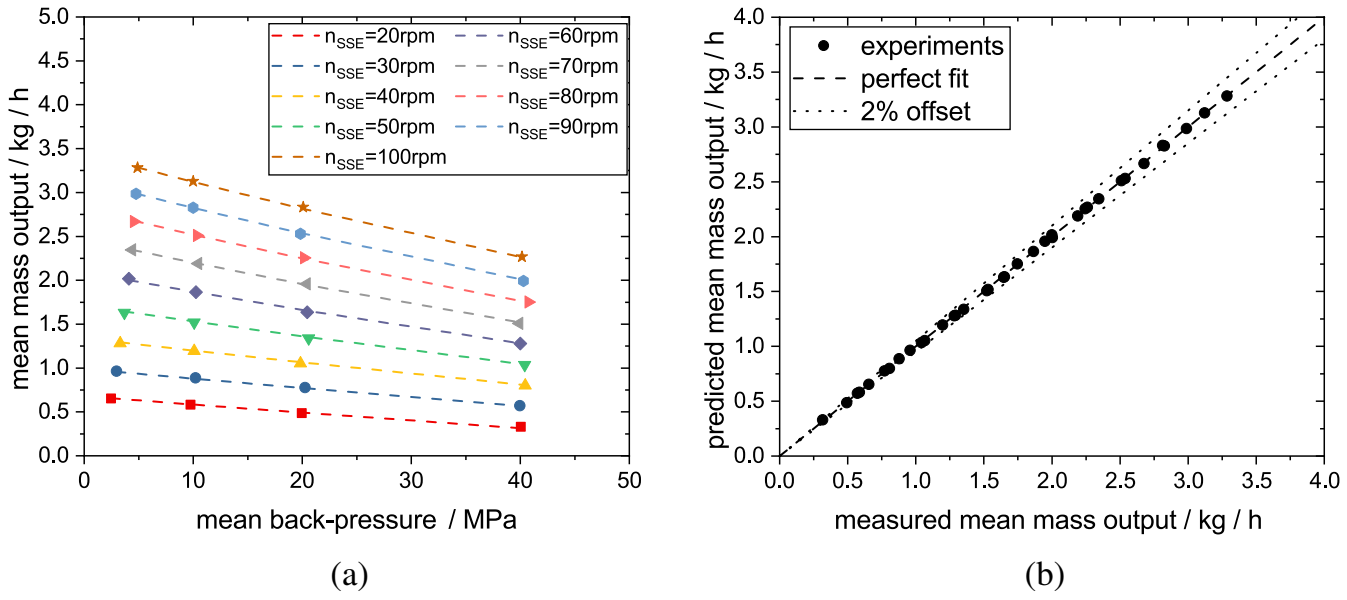


**FIGURE A1** | (a) Screw characteristic curve for PE-HD at 240°C. Dashed lines and symbols show the results of the heuristic model and the experiments, respectively. (b) Measured vs. predicted mass output (heuristic model at 240°C). Circles mark the experiments, the dashed line represents a perfect fit of $R^2 = 1$, and the dotted lines indicate a 2% offset from the perfect fit.

## Appendix B

### Additional Figures

The pressure-throughput behavior of the remaining materials is shown in Figures A1 and B1.

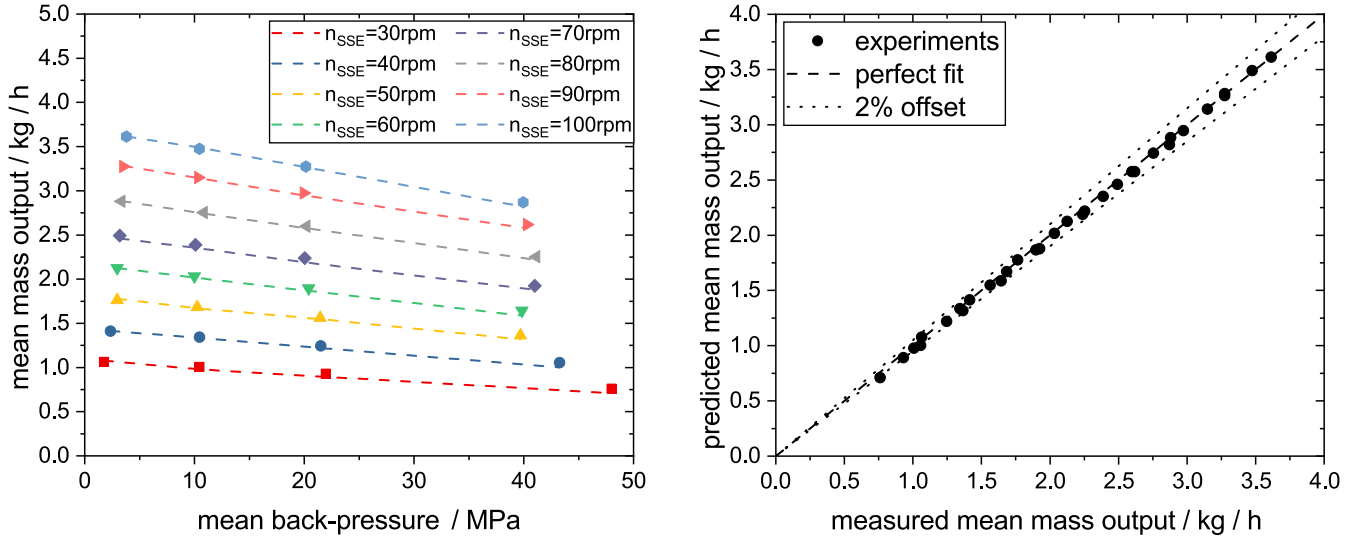


(a) (b)

**FIGURE B1** | (a) Screw characteristic curve for PE-LD PCR at 200°C. Dashed lines and symbols show the results of the heuristic model and the experiments, respectively. (b) Measured vs. predicted mass output (heuristic model at 200°C). Circles mark the experiments, the dashed line represents a perfect fit of $R^2 = 1$, and the dotted lines indicate a 2% offset from the perfect fit.